Comparison of Boeing 777 Landing Gear Noise Simulations with Flight Test Data

Michael Czech[1], Leon Brusniak[2]
The Boeing Company, Mukilteo, WA, 98275, USA

Mehdi R. Khorrami[3]
NASA Langley Research Center, Hampton, VA, 23681, USA

and

Ehab Fares,[4] Benedikt König[5]
Dassault Systèmes Deutschland GmbH, D-70563, Stuttgart, Germany

Acoustic phased microphone array measurements of aircraft flyover noise acquired during the 2005 Quiet Technology Demonstrator II test were used to assess the accuracy of high-fidelity, full-scale simulations of landing gear noise produced by a large civilian aircraft. The simulations, conducted with the lattice Boltzmann solver PowerFLOW®, used a highly accurate digital model of a Boeing 777-300ER aircraft with the nose and main landing gear components replicating the full-scale geometries. The simulations were performed for aircraft parameters that matched those recorded during the flyover test conditions. For benchmarking purposes, several aircraft configurations were simulated: a) nose landing gear deployed with main landing gear and wing high-lift devices stowed, b) nose and main landing gear deployed with wing high-lift devices stowed and c) nose and main landing gear with wing high-lift devices deployed. To facilitate direct comparison with measured data, the simulated data sets were used to generate synthetic pressure records at the same array microphone locations as those used during the flight test. Broadly self-consistent beamforming techniques and procedures were used to process the synthetic pressure records and the measured data. Integration of select regions of the beamform maps containing the nose or main landing gear yielded good agreement between predicted and measured integrated far-field spectra for forward directivity angles where airframe noise is more prominent.

I. Introduction

Landing gears generate a significant portion of the airframe noise produced by large commercial aircraft [1-4]. In general, the quantification and assessment of landing gear noise – an intrinsically complex process – ranges from empirical scaling formulas based on existing data sets, to wind-tunnel experiments at subscale, to flight testing. While wind-tunnel experiments are an efficient method for assessing novel noise reduction technologies and providing an overall understanding of landing gear noise, the inherent limitations in geometric fidelity and local flow conditions make extrapolation of subscale noise levels to those of an installed, full-scale gear difficult. System-level, accurate, full-scale prediction of landing gear noise for large aircraft is a daunting task because of the extreme range of physical scales and geometric complexity of the relevant components, which gives rise to a flow field that contains a broad range of spatio-temporal scales. Computational approaches that can provide an efficient assessment of full-scale

---

[1] Acoustic Engineer
[2] Acoustic Engineer, currently independent acoustic consultant
[3] Senior Scientist, Computational AeroSciences Branch, Associate Fellow AIAA.
[4] Director, Aerospace and Defense (currently with Geely Auto Technical, Deutschland, GmbH), Senior Member AIAA.
[5] Senior Specialist, SIMULIA, Aerospace & Defense.

landing gear noise have made significant strides toward achieving this grand challenge within the aerospace community. A critical aspect of this challenge is the validation of numerically computed results while simultaneously ascertaining the predictive capability of the computational approach to identify shortcomings and deficiencies to be remedied in the future.

Building upon the advances made under the NASA Environmentally Responsible Aviation and Flight Demonstrations and Capabilities (FDC) projects, the NASA-Boeing joint effort on airframe noise prediction (2016 – 2020) was created to extend simulation-based methodology to the landing gear and high-lift systems of full-scale, large civil transports. Based on the availability of model- and full-scale aeroacoustic measurements, a high-fidelity representation of a Boeing 777 (B777) aircraft was used in the simulations. The multi-year collaboration comprised several phases. To determine the efficacy of, and build confidence in, the applied computational methodology, the initial phases consisted of carefully planned simulations and validations of a high-fidelity, 26%-scale main landing gear model of a B777-200 aircraft, installed with a wing and in isolation. The successes of these initial computational studies, documented in Refs. [5-8], paved the way for the much more challenging computations of a full-scale, complete aircraft. The full-scale simulation effort was executed in various stages of increasing geometrical complexity from a single nose gear with a coarser representation of an airplane in a cruise configuration through deployment of additional airframe components. To gain deeper insight and ensure a successful outcome, three aircraft configurations, namely a) nose landing gear (NLG) deployed with main landing gear (MLG) and wing high-lift devices stowed (NLG-only), b) nose and main landing gear deployed with wing high-lift devices stowed (Config1), and c) nose and main landing gear and wing high-lift devices deployed (Config2, landing configuration), were selected for full-scale simulation.

Simulations of the full-scale, installed NLG of a B777-300ER aircraft in combination with a cruise wing were performed first to address several important issues. We know from past experience [9] that, because of its forward location away from other airframe components, the noise produced by the NLG is essentially unaffected by the presence of the MLG and/or high-lift devices. As a result, the setup for the isolated NLG enabled simulations at a very fine spatial resolution that would have been prohibitive if the MLG were also deployed. By performing the NLG-only simulations at successively finer resolutions, we were able to ascertain the full effect of spatial resolution on predicted sound levels and frequency content of the far-field spectrum. The insights and experience gained from the NLG-only simulations were instrumental in guiding the development of a tailored meshing strategy better suited for the extremely challenging simulation of Config1 and Config2. The computational effort on the full-scale, isolated NLG is described in Ref. [10].

The present paper focuses on comparing the simulated, radiated acoustic field on the ground generated by a B777-300ER with acoustic data acquired during the 2005 Quiet Technology Demonstrator II (QTD2) flight test campaign [4, 11]. The present benchmarking effort targeted NLG and MLG far-field noise signatures and used the computational data obtained from simulations of configurations NLG-only, Config1, and Config2 [10, 12]. Detailed accounts of the geometry development, simulation setup, and computed aeroacoustic trends for the latter two configurations are provided in Ref. [12].

II. Experimental and Computational Data Sets

The experimental data consist of flush dish ensemble array and phased array measurements for Config1 and Config2 extracted from the flights that were exclusively dedicated to airframe noise during the 2005 QTD2 test [11]. An All Nippon Airways B777-300ER served as the test aircraft. The Boeing phased array comprised of 614 microphones arranged in a multi-arm, logarithmic spiral pattern laid out on a 300 ft by 250 ft area (Fig. 1). Each data acquisition instance lasted approximately 16 seconds. Flight test speed and flight path angle were held approximately constant during that period. All microphone channels were simultaneously sampled at 102.4 kHz. Descriptions of the flight test, noise reduction concepts evaluated, and array measurements are given in Refs. [4, 11, 13]. The ensemble array consisted of 8 microphones that were ensemble averaged to provide absolute measurements of the total far-field aircraft noise signature over the required range of emission angles. The derived total phased array levels were then normalized to the overall noise levels determined by the flush dish microphones.

The computational data were generated during an extensive simulation campaign of the full-scale B777-300ER aircraft [10, 12] for configurations NLG-only (Fig. 2), Config1 (Fig. 3a), and Config2 (Fig. 3b). Note from the figures that the NLG-only configuration does not include flap bracket fairings – when the flaps are stowed, these fairings do not generate noise. The flight conditions and aircraft parameters selected for the simulations (Table 1), except for the Reynolds number (Re), matched those recorded during two array flyover passes that were executed to the same target conditions. The Re for all computations was 20×10^6, which is approximately 35% and 50% of the flight Re based on mean aerodynamic chord and the aircraft speeds of Table 1 for Config1 and Config2, respectively. This Re is sufficiently high to produce far-field noise levels that are nearly equivalent, but at a lower computational cost, to those obtained at full flight Re. Detailed discussions on Re effects can be found in Refs. [12, 14]. All simulations were performed with the lattice Boltzmann solver PowerFLOW® to capture time-dependent flow data. An overview of mesh characteristics for the various spatial resolutions and configurations simulated for this study is given in Table 2. Note that the finest voxel edge length – used to resolve the smallest geometrical structures – was reduced by a factor of 1/1.5 between resolution levels. We note also that, while the same finest grid resolution was employed for all three configurations, more of the geometric details of the gear in the NLG-only configuration were resolved because the finest mesh was applied to most of the nose gear surfaces. For Config1 and Config2, the finest spatial resolution was applied only to certain areas of interest around the NLG and MLG to limit computational costs.

Table 1. Flight conditions used for simulation of selected aircraft configurations.

Configuration	Angle-of-Attack (AOA)	Mach	Speed (kts)	Re
NLG-only, Config1	6.5°	0.344	229.8	20×10^6
Config2	4.0°	0.254	168.9	20×10^6

Table 2. Simulation parameters for NLG-only, Config1 and Config2.

	Resolution							
	Extra coarse			**Coarse**			**Medium**	**Fine**
Reynolds Number	20×10^6			20×10^6			20×10^6	20×10^6
Minimum cell size [mm]	1.4			0.94			0.62	0.42
Timesteps (for 2.5s) [10^6]	1.06			1.59			2.38	3.57
Geometry	**NLG-only**	**Config1**	**Config2**	**NLG-only**	**Config1**	**Config2**	**NLG-only**	**NLG-only**
Voxels [10^6]	860	2553	5030	2100	7324	14100	6400	20000
Surfels [10^6]	60	119	188	104	195	317	191	365
CPUh [1k]	80	255	1160	350	669	2921	1500	4500

Far-field pressure records at the phased array microphone locations were computed using a Ffowcs-Williams and Hawkings (FWH) integral approach [15], with flow quantities on a permeable data surface enclosing the prominent noise source regions of interest used as input. Although very expensive computationally, the choice of a permeable data surface was based on studies [5, 10] demonstrating that significant inaccuracies in predicted far-field noise spectra exist when solid surface data are used as input. The shape and extent of the permeable data surfaces used for configurations NLG-only, and Config1 and Config2 are shown in Fig. 4 and Fig. 5, respectively. For the simulations involving Config1 and Config2 (Fig. 5), the entire aircraft should be, ideally, enclosed within the permeable data surface. Doing so, however, would produce prohibitively large grids and extremely high computational costs, or limit the simulations to the capture of only very low-frequency acoustic behavior. The merits of, and the process used to determine, permeable data surfaces are fully described in Refs. [10, 12]. The end caps placed at the exit plane of the permeable data surfaces are used, through end-cap averaging, to reduce the adverse impact of hydrodynamic fluctuations exiting the permeable surface. The synthetic microphone array pressure records contain approximately 0.8 s of simulated physical time, a period with sufficient samples to conduct statistically meaningful spectral analyses.[6]

[6] Experimentation with record lengths for Config1 revealed that differences in far-field noise spectral levels between 0.3 s, 0.5 s, and 0.865 s were insignificant, indicating that good convergence was achieved for record lengths greater than 0.4 s.

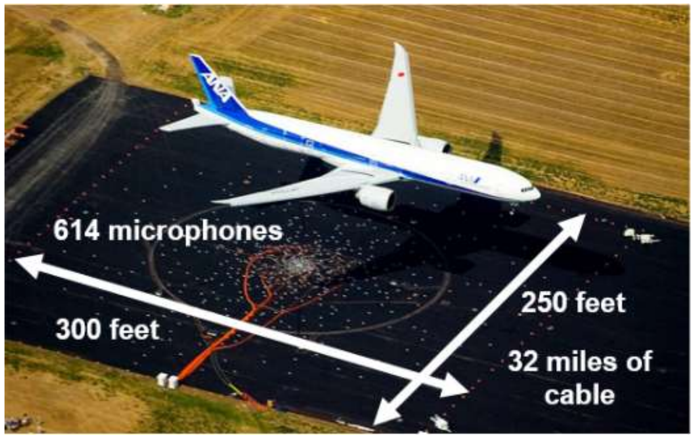

Fig. 1 All Nippon Airways Boeing 777-300ER flying over phased microphone array during QTD2 flight test (from Ref. [4]).

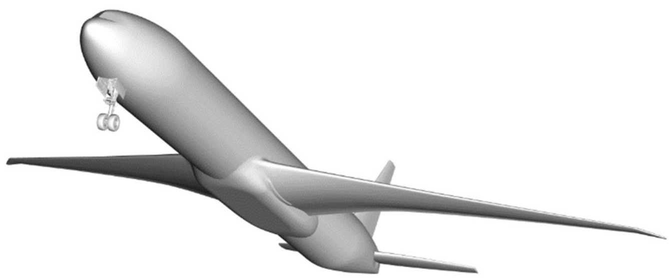

Fig. 2 Installed, isolated full-scale B777-300ER nose landing gear configuration (NLG-only, from Ref. [10]).

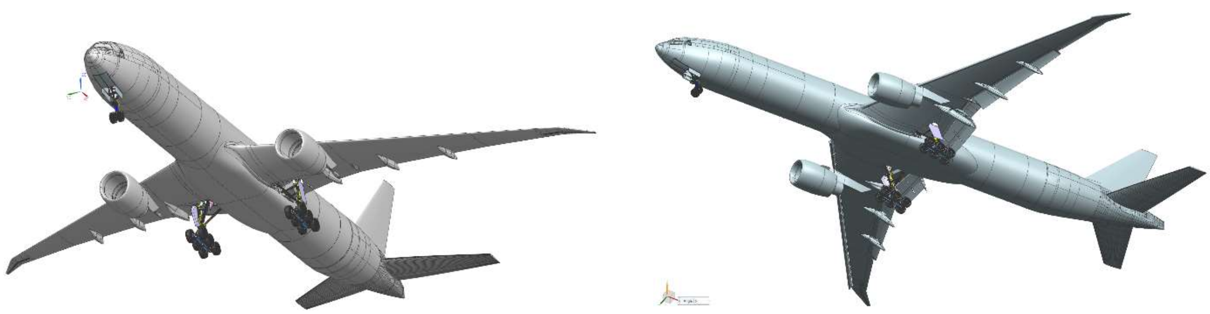

a) High-lift devices stowed (Config1) **b) High-lift devices deployed (Config2)**

Fig. 3 Full-scale B777-300ER aircraft with nose and main landing gear deployed (from Ref. [12]).

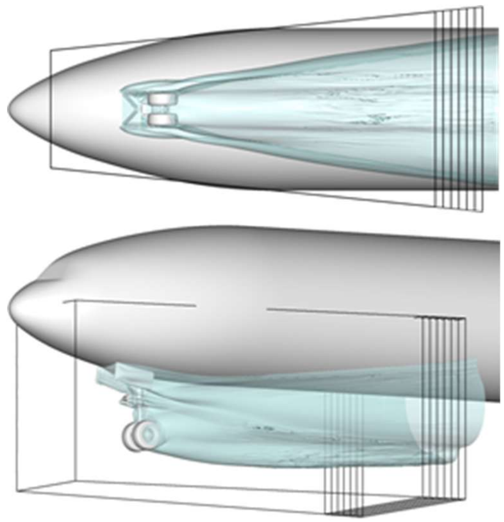

Fig. 4 Permeable FWH data surface (identified by gray lines) used for propagating nearfield pressures to the far field (from Ref. [10]).

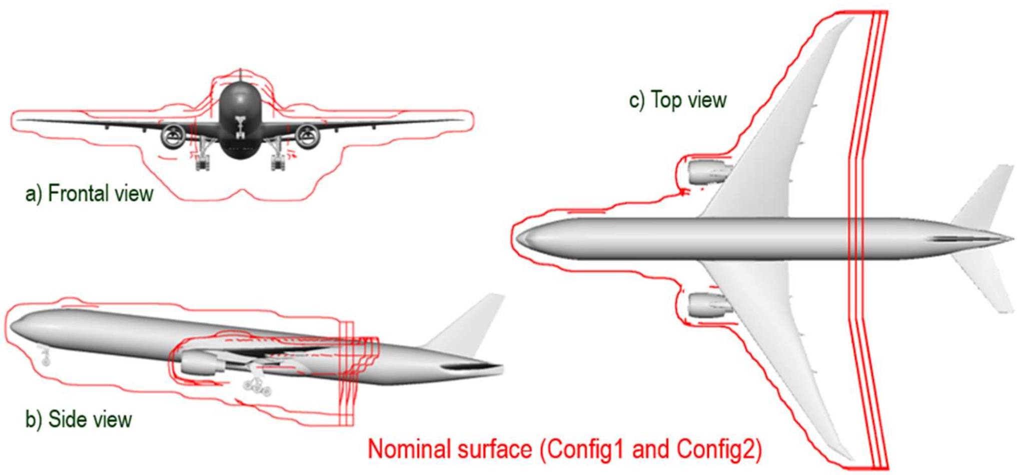

Fig. 5 Permeable data surface for Config1 and Config2 (red line) used for far-field noise computations (from Ref. [12]).

A. Data Analysis

The objective of the analysis was to obtain aircraft noise subcomponent spectra - from both the airplane flyover test and the numerical simulations - that could be used to directly evaluate the capabilities of the present computational approach for predicting noise source strength and far-field acoustic signatures of landing gear components. A straightforward, direct comparison would be to use physical flyover calibrated ground ensemble array microphone levels and the analogous levels provided by the simulation. Of course, an even more rigorous comparison could be possible only if 1) all geometric details of the landing gear and high-lift components, including slat and flap brackets, corresponded to those flown on the actual aircraft; 2) residual engine noise – always present with engines operating at flight-idle conditions and thus included in the measured pressure records – were accounted for in the simulations; 3) the effects of time-dependent atmospheric conditions present during the test could be included in the simulations; and 4) the simulation data would account for airplane motion to capture the range of emission angles over which the aircraft flew in the process of acquiring data for the target emission angle (here, the simulations utilized an airplane fixed in position relative to the phased array microphone locations, as opposed to the airplane position continuously changing with time as in the actual flyover). Although the simulations did not benefit from as-flown slat and flap bracket geometries and did not include residual propulsive noise, they provided data for a meaningful evaluation of the computational approach. To fulfill the objective of the analysis, physical flyover aircraft subcomponent noise levels were extracted using acoustic phased array processing methods. For comparative purposes, analogous subcomponent spectra were required from the simulation. This necessitated the paradigm of applying array signal processing methods to the synthetic pressure records obtained from Computational Aeroacoustics (CAA) simulations, the first application of this concept having been that of Ref. [16] for the large eddy simulation of a jet flow. In that study, the authors recognized that data from such applications of phased array processing methods represented an "ideal acoustic phased array", where self-noise of the system (e.g., electronic noise, background noise) is zero, and the frequency response at each simulated array "sensor" is unity across all frequencies.

Because of the legacy nature of the QTD2 array results and differences between flight test and simulation setups, the measured and synthetic pressure records were processed differently. The physical flyover data were processed using time-domain conventional beamforming (Ref. [17]) to create source localization (beamform) maps, which were then deconvolved using the DAMAS2 method of Ref. [18] in order to remove the effects of convolution of the array point spread function with the noise sources. Subcomponent noise levels were extracted from the deconvolved maps and summed together, this total then being matched to the calibrated ground ensemble array microphone levels to provide calibrated phased array subcomponent levels. Note that the beamforming grid in this case encompasses the entire aircraft. This phased array data extraction process is described in detail in Ref. [19].

The time-dependent flow quantities collected on the permeable data surface, in conjunction with the FWH propagation approach described in Ref. [15], were used to obtain the time histories of the fluctuating pressures at the same relative microphone locations as those used during the flight test. Unlike the physical flyover where the aircraft is in continuous motion relative to the phased array microphones, the aircraft and microphones in the simulation are fixed in space relative to each other over the course of the simulation: the simulation is analogous to a wind tunnel experiment in which source and receiver are fixed in space relative to each other during the course of measurement. The simulation data were, therefore, processed using frequency domain conventional beamforming. In an effort to substantially reduce array processing time and directly compare the experimental DAMAS2 integration results to the simulation conventional beamforming results, the simulation subcomponent noise levels were obtained by accounting for array effects (i.e., by subtracting the point spread function – centered in the middle of the map – from the map) and then integrating over the defined subcomponent region. Whereas deconvolution was used for the physical flyover processing, the point spread function subtraction method was used for the simulation processing owing to time and budget constraints. This small discrepancy in the array processing approach is expected to have negligible effect on the spectral levels based on unpublished work using wind tunnel data. For comparisons with measured phased microphone array data, atmospheric effects were taken into account through appropriate corrections applied to the CAA simulation results. Fig. 6 provides a nose landing gear conventional beamform map at 630 Hz from both the flight test and simulation, where the beamforming grid passes through the aircraft reference location (the center point between the in-flight main landing gear truck middle wheel rotation axes) and is parallel to the aircraft centerline axis. The beamform noise maps are seen to be quite similar.

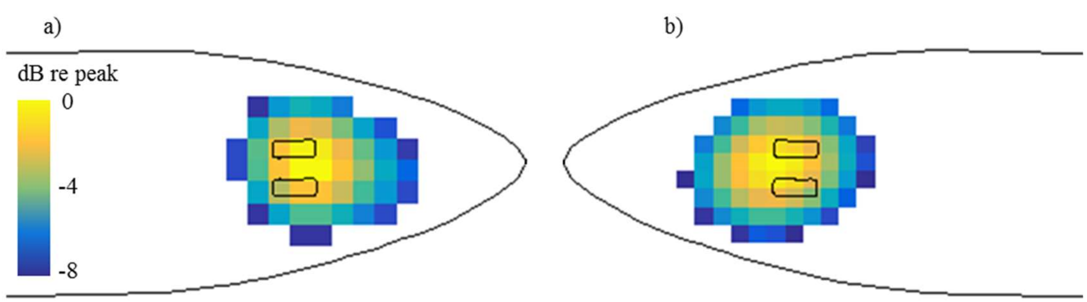

Fig. 6 Comparison of nose gear beamform maps at 630 Hz and 90° emission angle for a) flight test and b) simulation.

For extraction of the landing gear noise subcomponents, comparable integration regions were defined for both the physical flyover and simulation data sets. For the nose gear, the region consisted of a single "box" centered on the gear. For the main landing gear, the integration region consisted of mirror-imaged boxes centered on the aircraft centerline encompassing the port and starboard main gear, with the beamforming grid passing through the aircraft reference location and being parallel to the aircraft centerline axis. Note that all directivity angles are specified relative to the aircraft reference location.[7]

[7] For directivity angles between 70° and 120°, the corresponding emission angles for the NLG would be 7°-10° higher, since this component resides substantially upstream of the MLG.

The physical flyover phased microphone array time series data were acquired at a time resolution of 9.766 μs. As per the method of Ref. [17], the time series data were resampled (after de-dopplerization) using a time resolution of 80 μs and the beamformed spectra were created using 512 points per Discrete Fourier Transform (DFT) block, resulting in a narrowband frequency resolution of 24.41 Hz. For the simulation timeseries data, the time resolution varied with grid resolution. In order to directly compare the integrated far-field spectra obtained from the measured and simulated beamform maps, the simulation cross-spectral matrices were created using DFT block sizes (number of points per DFT block) that allowed as close a matching as possible to the flyover data spectral resolution of 24.41 Hz. This was done to ensure that conversion of narrowband data to 1/3 octave band data utilized the same corresponding narrowband bins per each 1/3 octave band in the reduction process for all simulation cases. On a final note, physical flyover data beamforming at each emission angle used a timeseries duration corresponding to the time over which the aircraft traveled a distance of 100 ft in the x direction (i.e. along the flight path). As per the speeds listed in Table 1, this resulted in phased array sampling durations at each emission angle of approximately 0.26 s and 0.35 s for NLG-only/Config1 and Config2, respectively.

III. Results and Discussion

In contrast to well-controlled, model-scale tests conducted in ground facilities, flight testing is subject to variations in atmospheric conditions, airplane performance, and test site environment (e.g., background noise). To reduce variability, flight tests are performed in a weather window that allows proper implementation of atmospheric attenuation corrections and permits tight control of airplane speed and flight path deviation. Nevertheless, some variability in the acquired noise spectra is unavoidable, and this may be somewhat greater than that obtained in a wind-tunnel experiment or in a static engine test. Prior to comparing the computational results with measurements, it was deemed informative to have an estimate of the pass-to-pass variation in the measured far-field noise signature of the NLG component only. This component was selected because of its position, isolated from other prominent airframe sources, whereby a well-defined integration region can be devised to yield the far-field noise spectrum without including residual noise from other sources. Fig. 7 shows the phased array-derived NLG spectra for five separate, but similar, flyover aircraft passes. The measured spectrum highlighted by the large symbols corresponds to the aircraft pass selected for simulation and posterior comparison with predicted results. Due to the similarity of the flyover conditions, it is reasonable to assume that the comparison in Fig. 7 shows a representative uncertainty of such measurements. From the plotted spectra, observe that for frequencies above 200 Hz the uncertainties may be broadly bound within a 2.5 dB range.

For modern, large commercial aircraft, airframe noise is a prominent component of total aircraft noise during approach and may dominate forward radiation in the flyover direction. During flight tests, the aircraft is closest to the ground array when it is overhead, at 90°. Thus, far-field spectra are less affected by atmospheric attenuation when obtained from integration of beamform maps that correspond to 90° and relatively close adjacent angles. The computational time and cost associated with the generation of synthetic array pressure records can be significant. For these reasons, only results at emission angles of 70°, 90° and 120° are presented in this section.

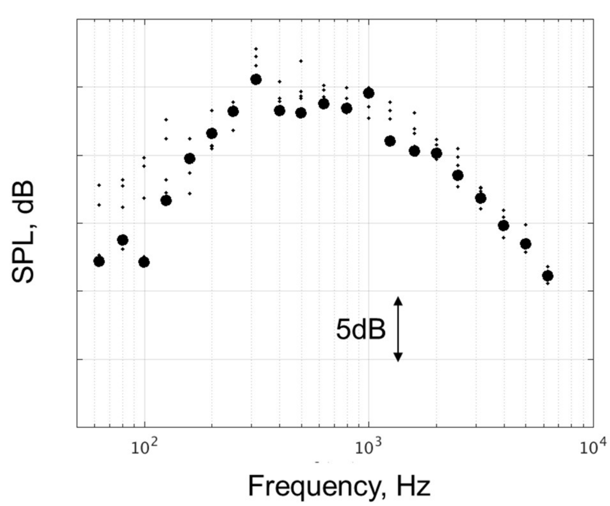

Fig. 7 Nose gear component flight test 1/3rd-octave spectra for several similar flyover conditions at 90° emission angle. The large symbols represent the condition modelled with CAA.

A. Comparison for the Isolated NLG

The nose gear component (NLG-only), simulated at a fine grid resolution, is compared to experimental data in Fig. 8 at emission angles of 70°, 90° and 120°. The results in Fig. 8 show excellent agreement at 70° and 90° for frequencies above 100 Hz; however the experimental data below about 200 Hz is believed to be somewhat less reliable. The roll-off of the nose gear spectra is captured well in the predictions. The comparison at 120° is less favorable, and the nose gear spectrum is under-predicted by approximately 2 to 3 dB over a wide frequency range. Although the experimental scatter is on the order of 2.5 dB, the disagreement between simulation and measurement is unlikely to be caused solely by data scatter. As will be seen in subsequent sections, the under-prediction of the spectral levels at the 120° emission angle is also present in the NLG and MLG data obtained from the simulations of Config1 and Config2. From a computational standpoint, there is nothing unique about aft emission angles. That is, given the good agreement achieved between measured and predicted spectra in the forward direction, similar agreement in the aft direction would be expected. However, one must be aware of certain factors, such as residual engine noise, that may contaminate the acoustic signature of the landing gear in the aft quadrant more significantly during passes of the aircraft over the ground array.

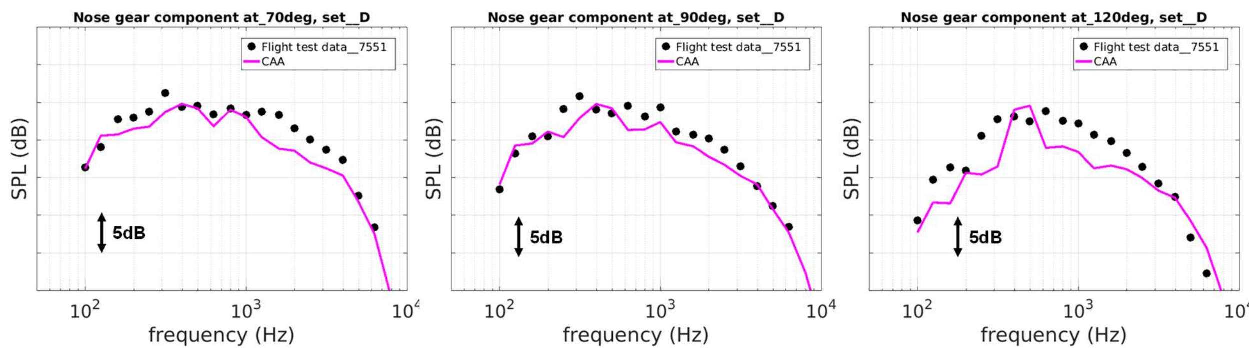

Fig. 8 Isolated nose gear (NLG-only) component prediction at fine spatial resolution compared to measurement.

A comparison of the computational results at different grid resolutions is provided in Fig. 9. Improved spatial resolution causes a distinct and expected increase in the simulated spectral levels at higher frequencies. While there is some variability at frequencies below 1 kHz, the variation tends to stay within 1 dB and is an implicit result of the better-resolved flow structures. The predicted trends may only be considered well-resolved up to about 1.5 kHz for the extra coarse grid; at higher frequencies, a spectral roll-off is clearly observed. Increments in grid resolution improve not only the spectral modeling of the finer spatial scales, but also the modeling of smaller flow features that also impact, to a lesser extent, the behavior of the larger flow features. This trend can be observed at all three emission angles shown here. Note also that the extra coarse grid resolution shows a very strong tone at 500 Hz and 120° that is not found in the experimental data or the finer grid resolution results. The presence of this tone points to a more fundamental challenge in numerical predictions, where under-resolution of certain flow interactions may result in unrealistic acoustic behavior and, in this case, the production of a strong tone. A variation in grid density is, therefore, always recommended as flow instabilities are very sensitive to both flow field and geometry details.

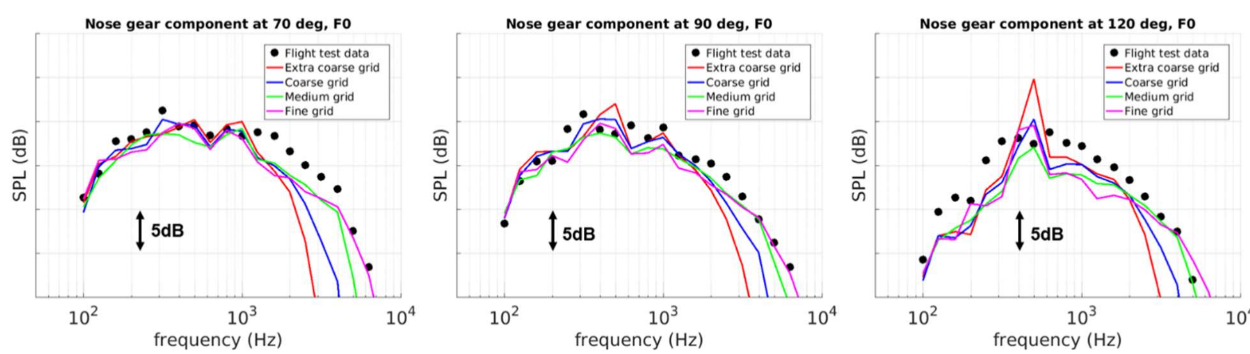

Fig. 9 Grid sensitivity results for the isolated nose gear component at flaps 0 (retracted high-lift system)

B. Main landing gear component predictions with the high-lift system retracted

As described in Ref. [12], due to the massive computational undertaking, the medium resolution simulations for Config1 and Config2 were ongoing when the NASA-Boeing joint effort ended. Thus, synthetic data were available for extra coarse and coarse resolution levels only. The predicted MLG spectrum, obtained from Config1 simulations, is compared to flight test data in Fig. 10. Overall, good agreement in the spectral shapes and levels was attained at the three emission angles considered.[8] The computational results tend to overpredict the experimental data at low and mid frequencies, but generally fall within the conjectured 2.5 dB uncertainty range of the QTD2 acoustic measurements. As expected, the higher spatial resolution grid provided a better estimate of the main gear component noise at higher frequencies. We fully anticipate that further grid refinement will extend the favorable comparison to frequencies above 2 kHz.

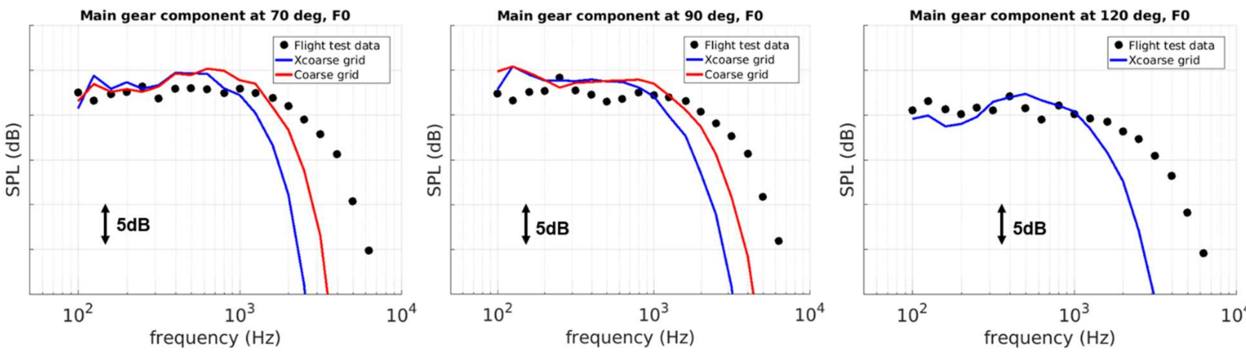

Fig. 10 Main gear component levels at flaps 0 (retracted high-lift system) for the extra-coarse (xcoarse) and coarse grid resolution

C. Nose and main landing gear component predictions with the high-lift system deployed

The second configuration being compared is a typical approach configuration with flaps (and slats) down and represents the most computationally challenging case. Fig. 11 shows the nose gear spectral component comparison at emission angles of 70°, 90° and 120°. The agreement is very good up to about 1.5 kHz, beyond which the grid resolution is insufficient to adequately resolve the acoustic waves, and the spectra drop off steeply. Note that the predictions seem to indicate a tonal feature at 1 kHz for the extra coarse grid results at an emission angle of 70° that is not found in the flight data. While the coarse grid results do not show this feature, a tone is found at this resolution at 400 Hz and 90°. Close examination of the NLG-only velocity and pressure fields indicated that the tone at 400 Hz resulted from the interaction of vortices shed by the toe bar with downstream structures of the NLG axle. As shown in Fig. 9, this tone diminished substantially with increased spatial resolution. Moreover, the flight test data displayed in Figs 3. 7, 8, and 9 also show a tone in the spectra, albeit at a lower frequency closer to 300 Hz. The difference in predicted vs. measured frequency for this tone could be attributed to the local flow conditions (e.g., presence of cross wind, atmospheric turbulence) during the aircraft pass over the array, which certainly were different than the ideal conditions used in the simulations. The flight test spectra at 120° are under-predicted by approximately 2 dB, as was also observed in the comparison for NLG-only (flaps retracted and higher flow speed). The comparisons are broadly similar to those for the nose gear component with flaps up (NLG-only). The results indicate a very favorable agreement between synthetic and experimental data trends for NLG noise over the wide speed differences between Config1 and Config2. Further, the best agreement occurs at the forward angle for which landing gear noise is more important.

[8] Coarse resolution pressure records at 120° emission angle could not be processed prior to conclusion of the NASA-Boeing joint effort.

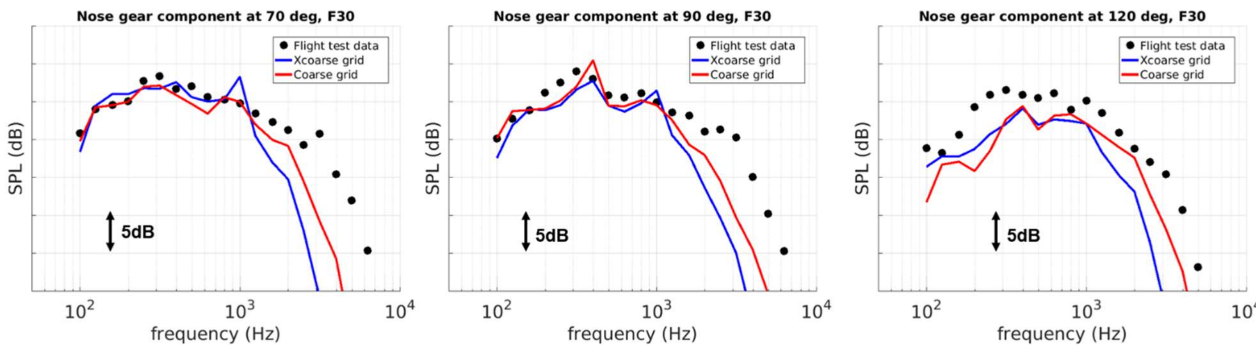

Fig. 11 Nose landing gear at flaps 30 (deployed high-lift system).

The main landing gear component comparisons in Fig. 12 illustrate an overall very good agreement between the coarse grid simulations and flight test data. The differences are typically within 2 dB up to about 2 kHz, beyond which the spatial resolution of the coarse grid becomes inadequate to capture the high frequency noise segment of the spectra. In addition, the agreement is of similar quality at all angles. Like the earlier findings, the increase in grid resolution has only a slight effect on the spectral levels below about 1 kHz.

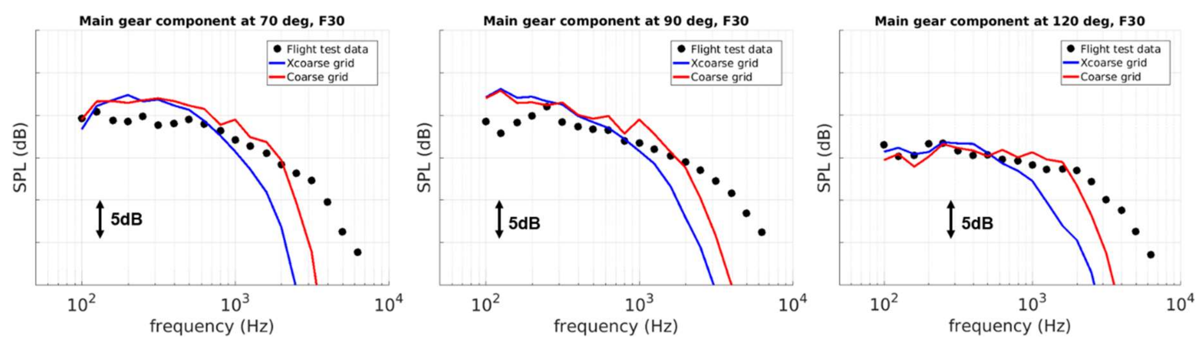

Fig. 12 Main landing gear component at flaps 30 (deployed high-lift system).

IV. Concluding Remarks

Detailed comparisons between full-scale simulations of a high-fidelity Boeing 777-300ER geometric model and acoustic measurements of airframe noise from the 2005 QTD2 flight test of the same aircraft have been presented here. The simulations, performed with the lattice Boltzmann solver PowerFLOW®, used digital representations of the nose and main landing gears that faithfully replicated the as-flown components. To facilitate validation of the predicted results, the simulations were performed for aircraft parameters that matched those recorded during select QTD2 flyover passes. To benchmark the present computational approach, simulations were conducted for several aircraft configurations at multiple grid resolutions. The configurations comprised a) nose landing gear deployed with main landing gear and wing high-lift devices stowed (NLG-only), b) nose and main landing gear deployed with wing high-lift devices retracted (Config1), and c) nose and main landing gear with wing high-lift devices deployed (Config2, landing configuration). Because of the lesser computational cost of the NLG-only simulations, successively finer grids – extra coarse, coarse, medium, and fine – were used to evaluate the effects of spatial resolution on the accuracy of the predicted sound levels and frequency content of the far-field spectrum. Due to the high computational requirements of Config1 and Config2, only results from the extra coarse and coarse spatial resolution grids were available for benchmarking purposes.

Microphone array measurements of aircraft flyover passes acquired during the QTD2 flight test were used to validate the computed noise levels and assess the predictive capability of the simulation approach. Comparison of the measured integrated far-field spectra of the NLG component with corresponding NLG-only simulated results indicated very good agreement at emission angles of 70° and 90° in the flyover direction. Solution accuracy improved greatly with increased (finer) spatial resolution, with fine grid results agreeing with flight test data up to 5 kHz–6 kHz, the highest frequencies measured. In contrast, the predicted spectra at the flyover emission angle of 120° noticeably underpredicted the measured spectrum over a significant frequency range. Increased spatial resolution failed to produce substantially better agreement. The predicted NLG noise trends observed in the aft quadrant were conjectured to be less influenced by spatial resolution issues than by factors such as residual engine noise in the measured acoustic data.

Comparisons of measured and predicted spectra for the MLG – obtained from Config1 simulations – demonstrated good overall agreement at the emission angles of 70°, 90°, and 120°. Similar to the NLG component, increased spatial resolution extended the range of good agreement to higher frequencies, with the coarse grid providing reasonably accurate spectral levels up to 2 kHz. The predicted far-field noise spectra for the NLG component of Config2 agreed well with measured levels at emission angles of 70° and 90°. The spectra at lower (extra coarse) resolution revealed the presence of tonal noise at approximately 1 kHz that is absent in the measurement. Increasing spatial resolution greatly diminished the tone, highlighting a fundamental challenge in numerical prediction: under-resolution of the flow field may produce incorrect acoustic behavior. As in the NLG-only case, Config2 NLG spectra significantly underpredicted QTD2 measured noise levels at the 120° emission angle. Comparisons of measured and simulated (Config2) spectra for the MLG displayed good agreement at the three emission angles considered. In general, coarse resolution noise levels were within 2 dB of the corresponding experimental data – well within the expected uncertainty band inherent in the QTD2 flight test measurements.

The overall good agreement between flight test and synthetic far-field noise spectra demonstrated in this study points to the great potential of CAA as an additional tool for the engineer when evaluating airframe noise. The simulations can provide great insight into the noise-generating mechanisms and thus guide research into the geometric modifications needed to achieve lower noise.

Acknowledgments

This work was supported by the FDC project under the Integrated Aviation Systems Program of the NASA Aeronautics Research Mission Directorate. We would like to express our sincere appreciation to personnel at the Boeing Company for their assistance with gathering and providing the CAD files of the as-flown nose and main landing gear geometries for a B777-300ER aircraft, in particular Navid Daneshvaran for meticulously resolving some of the geometry questions for the main landing gear. The authors also gratefully acknowledge the invaluable contribution of Scott Brynildsen of Craig Technologies for providing geometry modifications and CAD support. All simulations were performed on the Pleiades supercomputer at the NASA Advanced Supercomputing (NAS) facility at Ames Research Center. The logistical support provided by NAS staff is greatly appreciated.

References

[1] Dobrzynski, W., "Almost 40 Years of Airframe Noise Research: What Did We Achieve," *J. Aircraft*, Vol. 47, No. 2, March-April 2010, pp. 353–367.

[2] Chow, L. C., Mau, K., and Remy, H., "Landing Gears and High Lift devices Airframe Noise Research," AIAA Paper 2002-2408, June 2002.

[3] Stoker, R., Guo, Y., Streett, C., and Burnside, N., "Airframe Noise Source Locations of a 777 Aircraft in Flight and Comparisons with Past Model Tests," AIAA Paper 2003-3232, May 2003.

[4] Elkoby, R., Brusniak, L., Stoker, R., Khorrami, M. R., Abeysinghe, A., and Moe, J.W., "Airframe Noise Results from the QTD II Flight Test Program," AIAA Paper 2007-3457, May 2007.

[5] Konig, B., Fares, E. Ravetta, P. A., and Khorrami, M. R., "A Comparative Study of Simulated and Measured Main Landing Gear Noise for Large Civil Transports," AIAA Paper 2017-3013, June 2017.

[6] Ravetta, P. A., Khorrami, M. R., Konig, B., and Fares, E., "Analysis of Simulated and Experimental Noise Sources of the Boeing 777 Main Gear Model via CLEAN in 3D," AIAA Paper 2018-3417, June 2018.

[7] Koenig, B., Fares, E., and Khorrami, M. R., "Aeroacoustic Study of a Subscale Large Civil Transport (STAR) Model – Part 1: Simulations," paper to be presented at the 27th AIAA/CEAS Aeroacoustics Conference in Washington DC, June 2021.

[8] Khorrami, M. R., Koenig, B., Fares, E., "Aeroacoustic Study of a Subscale Large Civil Transport (STAR) Model – Part 2: Validation of Simulated Results," paper to be presented at the 27th AIAA/CEAS Aeroacoustics Conference in Washington DC, June 2021.

[9] Duda, B., Ferris, R. J., and Khorrami, M. R., "Simulation-Based Assessment of a Full-Scale Installed Quiet Landing Gear," AIAA Paper 2019-2476, May 2019.

[10] Fares, E., Koenig, B., and Khorrami, M. R., "Effect of Geometric Granularity on the Noise Signature of a Full-Scale Large Civil Transport Nose Landing Gear," paper to be presented at the 27th AIAA/CEAS Aeroacoustics Conference in Washington DC, June 2021.

[11] Herkes, W. H., Olsen, R. F., and Uellenberg, S., "The Quiet Technology Demonstrator Program: Flight Validation of Airplane Noise-Reduction Concepts," AIAA Paper 2006-2720, May 2006.

[12] Khorrami, M. R., Koenig, B., Fares, E., Ribeiro, A. F. P., Czech, M., and Ravetta, P., "Airframe Noise Simulations of a Full-Scale Large Civil Transport in Landing Configuration," paper to be presented at the 27th AIAA/CEAS Aeroacoustics Conference in Washington DC, June 2021.

[13] Brusniak, L. Underbrink, J., and Stoker, R. W., "Acoustic Imaging of Aircraft Noise Sources Using Large Aperture Phased Arrays," AIAA Paper 2006-2715, May 2006.
[14] Fares, E., Duda, B., and Khorrami, M. R., "Airframe Noise Prediction of a Full Aircraft in Model and Full Scale Using Lattice Boltzmann Approach," AIAA paper 2016-2707, May-June 2016.
[15] Ffowcs Williams, D. L. and Hawking, J. E., "Sound Generation by Turbulence and Surfaces in Arbitrary Motion," *Philosophical Transactions of the Royal Society of London, Series A, Mathematical and Physical Sciences,* Vol. 264, No. 1151, 1969, pp. 321–342.
[16] Brusniak, L., Shur, M., and Spalart, P., "Phased-Array Imaging of Jet Noise Sources in a Large-Eddy Simulation," AIAA Paper 2006-2444.
[17] Howell, G. P., Bradley, A. J., et al., "De-Dopplerization and Acoustic Imaging of Aircraft Flyover Measurements," Journal of Sound and Vibration, 105 (1), pp. 151-167, 1986.
[18] Dougherty, R. P., "Extensions of DAMAS and Benefits and Limitations of Deconvolution in Beamforming," AIAA Paper 2005-2961, May 2005.
[19] Brusniak, L., Wong, J. W., Nesbitt, E. H., Jones, M. G., and Nark, D. M., "Acoustic Phased Array Quantification of Quiet Technology Demonstrator 3 Advanced Inlet Liner Noise Component," AIAA Paper 2019-2765, May 2019.